Supplementary Information (SI) for ChemComm.
This journal is © The Royal Society of Chemistry 2024

Electronic Supporting Information

Manipulating Fe(II) Spin States to Achieve Higher Anti-tumor Cell Activities in Multinuclear Complexes

Nian-Tao Yao[a*], Qiang Liu[d], Jun-Wei Ma[c*], Xiu-Mei Du[a], Jing Ru[a], Jiao-jiao Jiang[a], Liang Zhao[b*], Yin-Shan Meng[b]

[a] Shandong Provincial Key Laboratory of Chemical Energy Storage and Novel Cell Technology, School of Chemistry and Chemical Engineering, Liaocheng University, Liao Cheng, 252000, China.
[b] State Key Laboratory of Fine Chemicals, Dalian University of Technology, Dalian 116024, China.
[c]School of Chemistry and Molecular Engineering, Qingdao University of Science and Technology, Qingdao, 266042, China.
[d]Instrumental Analysis Center, Dalian University of Technology, Dalian, 116024, China

Corresponding author: yntdlut@163.com; zhaoliang716@dlut.edu.cn; majw15@lzu.edu.cn

Contents

Experimental Section

Materials and Methods. The reagents and solvents employed in this study were procured at analytical purity levels from reputable commercial suppliers and were utilized without additional purification steps. The ligands, namely *N*-benzyl-*N*, *N*', *N*'-tris(2-pyridylmethyl) ethylenediamine (Bztpen) and *N*-benzyl-*N*, *N*', *N*'-tris(2-pyridylmethyl) propylenediamine (Bztppn), were synthesized following established procedures outlined in the literature.[1]

$\{Fe^{II}_2(Bztpen)_2[(Pd^{II}(CN)_4]_2\}\cdot 2H_2O$ (**1**) was synthesized by a diffusion method in an H–shaped test tube. A 2 mL solution of $Fe(ClO_4)_2\cdot 6H_2O$ (7.3 mg, 0.02 mmol) was placed at the bottom of one side of an H-type tube. A mixture of H_2O/MeOH (*v*/*v* = 1:1, 2 mL) solution of Bztpen (8.47 mg, 0.02 mmol) and $K_2[Pd(CN)_4]\cdot xH_2O$ (5.77 mg, 0.02 mmol) was placed in another side of the H-type tube. Then the MeOH solution as a buffer was carefully added to the top of the H-type tube. After six weeks without disturbing, red-brown plate crystals suitable for single-crystal X-ray diffraction were collected (yield ≈ 31.4 % (8.89 mg), based on the $Fe(ClO_4)_2\cdot 6H_2O$). Elemental analysis (%) calculated for $C_{62}H_{62}Fe_2N_{18}O_2Pd_2$: C 52.60, H 4.41, N 17.81; found: C 52.95, H 4.56, N 18.27.

$\{Fe^{II}_2(Bztppn)_2[(Pd^{II}(CN)_4]_2\}\cdot 2H_2O$ (**2**) were prepared in a similar way to 1 but using Bztppn. Yield: ≈ 25.8 % (7.45 mg) based on the $Fe(ClO_4)_2\cdot 6H_2O$ Elemental analysis (%) calculated for $C_{64}H_{66}Fe_2N_{18}O_2Pd_2$: C 53.24, H 4.61, N 17.46; found: C 53.67, H 4.79, N 17.95.

Physical measurements. The single-crystal XRD data for **1** were collected on Bruker D8 Venture CMOS–based diffractometer (Mo–Kα radiation, λ = 0.71073 Å) using the SMART and SAINT programs. Final unit cell parameters were based on all observed reflections from the integration of all frame data. The structures were solved with the ShelXT structure solution program using Intrinsic Phasing and refined with the ShelXL refinement package using Least Squares minimization that was implanted in Olex2. Magnetic measurements of samples were performed on a Quantum Design SQUID

(MPMS XL–7) magnetometer. Measurements were performed using polycrystalline samples by the parafilm with polycarbonate capsules. Data were corrected for the diamagnetic contribution calculated from Pascal constants and background from the parafilm and capsules.

Stability of complexes in DMSO and PBS:

To assess the stability of complexes **1** and **2** in DMSO and PBS, the UV-Vis absorption were conducted. The complexes were dissolved in DMSO at a concentration of 2.4 μM, then dispersed in PBS (V_{DMSO}:V_{PBS} = 2:3) and placed in a 1 cm quartz cell for UV-Vis analysis. Additionally, the effect of ethanethiol on the stability of the complexes in DMSO was also examined by dissolving the complexes and ethanethiol in DMSO at a molar ratio of 1:50.

MTT assay. The cervical carcinoma cell line (HeLa) and hepatocellular carcinoma cell line (HepG-2) were cultured in DMEM (Gibco) medium at 37 ^{o}C with 95% air and 5% CO_2. Seeded at a density of 10^5 cells/mL in 96-well plates, the cell lines underwent a 24-hour incubation in a complete growth medium. The cells were treated with the complexes **1** and **2** for 24 hours. Then, a fresh solution of 3-(4,5-dimethylthiazol-2-yl)-2,5-diphenyltetrazolium bromide (MTT) (0.5 mg/mL) was added to each well of the 96-well plates, and the plate was incubated in a CO_2 incubator for 4 h. The cells were dissolved with 100 μL of DMSO and analyzed in a multiwell-plate reader (Bio-Rad iMark) at 490 nm.

Cell apoptosis assay with flow cytometry (FCM). HepG-2 cells were plated in six-well plates and incubated for 24 hours to allow exponential growth, then treated with test complexes for 24 hours. The treated cells were collected and labeled with FITC-Annexin V/PI apoptosis detection kit (BD pharmacy Biosciences, USA) according to the manufacturer's protocol. Cell apoptosis was quantified by flow cytometry (guava easyCyte) analysis.

Intracellular ROS assay with DCFH-DA staining. Intracellular ROS levels were determined by oxidation sensitive probe 2',7'-dichlorofluorescein fluorescence (DCFH-DA). HepG-2 cells were plated in a six-well plate and treated with complex **1**

for 6 hours, and then stained with DCFH-DA (10 μM) for 30 min at 37 °C. Following incubation, the cells were washed twice with PBS and analyzed immediately for the green fluorescence intensity with flow cytometry and laser confocal microscopy. When necessary, the cells were pretreated with NAC (1 h) before adding the test complex.

Analysis of mitochondrial membrane potential. HepG-2 cells grown for 24 hours in six-well plates were treated with or without complex **1** for 24 h to obtain the control and treated cells, respectively. The control and treated cells were harvested, and 5,5′,6,6′-tetrachloro-1,1′,3,3′-tetraethylbenzimidazolyl phthalocyanine iodide (JC-1, Molecular Probes, Eugene, OR) probe was added to stain the cells. The MMP was detected by flow cytometry and laser confocal microscopy according to experimental requirements.

Evans' method[2,3]

Magnetic susceptibility data of the solution were acquired at room temperature using ^{1}H NMR spectroscopy on a Bruker 500 MHz spectrometer, following the literature procedure employing Evans' method. Samples of pure complexes **1** (4.0 mg) and **2** (2.5 mg) were dissolved separately in 1 mL of DMSO-d_6. A capillary insert containing pure DMSO-d_6 was positioned within the outer tube, which held the sample solution. The calculation equation is provided below:

$$\chi_M T = (\frac{3\Delta f}{4\pi m f} M + \chi_M{}^{dia}) \times T$$

Where m is the concentration of the paramagnetic solution in g mL^{-1}, f is the spectrometer frequency in Hz, Δf is the shift of the DMSO-d_6 peak in the paramagnetic solution compared to pure DMSO-d_6 in Hz. $\chi_M{}^{dia} = M \times 10^{-6}$ cm^3 mol^{-1} (M is the molecular weight).

References

[1] L. Duelund, R. Hazell, C. J. McKenzie, et al. *J. Chem. Soc., Dalton Trans.*, 2 (2001), 152–156.

[2] D. F. Evans, *J. Chem. Soc.* **1959**, 2003-2005.

[3] C. Yi, Y.-S. Meng, L. Zhao, et al., *CCS Chemistry*, 5 (2023) 915-924.

Table S1. Crystal data and structure refinements for complexes **1** and **2**

Complexes	**1**$^{295\ K}$	**2**$^{250\ K}$	**2**$^{70\ K}$
Formula	$C_{62}H_{62}Fe_2N_{18}O_2Pd_2$	$C_{64}H_{66}Fe_2N_{18}O_2Pd_2$	$C_{64}H_{66}Fe_2N_{18}O_2Pd_2$
CCDC	2344518	2344516	2344517
Fw	1415.79	1443.84	1443.84
Crystal system	Monoclinic	Monoclinic	Monoclinic
Space group	$P2_1/c$	$P2_1/c$	$P2_1/c$
a (Å)	9.2363(9)	9.4476(3)	9.3591(2)
b (Å)	18.5613(18)	18.2347(8)	18.1555(5)
c (Å)	17.5151(18)	18.4506(7)	17.8670(4)
α (°)	90	90	90
β (°)	100.831(13)	103.4850(10)	101.7750(10)
γ (°)	90	90	90
V (Å^3)	2949.3(5)	3090.9(2)	2972.06(12)
Z	2	2	2
ρ_{calc} (g/cm^3)	1.594	1.551	1.613
F (000)	1440	1472	1472
Reflections collected	59692	57577	22320
Unique reflections (R_{int})	0.0473	0.0477	0.0361
Goodness–of–fit on F^2	1.061	1.025	1.020
R_1 [$I>2\sigma(I)$][a]	0.0312	0.0317	0.0331
wR_2 [$I>2\sigma(I)$][b]	0.0671	0.0702	0.0697

[a] $R_1 = \Sigma\ (|F_O|-|F_C|) / \Sigma\ |F_O|$; [b] $wR_2 = [\Sigma\ w\ (|F_O|-|F_C|)^2 / \Sigma\ w\ F_O^2]^{1/2}$

Table. S2 Selected bond distances (Å) and angles (°) for **1** at 295 K.

Complex **1**[295 K]			
Fe(1)-N(1)	1.9172(19)	Fe(1)-N(4)	2.0005(18)
Fe(1)-N(2)	1.979(2)	Fe(1)-N(5)	1.9964(19)
Fe(1)-N(3)	1.9568(19)	Fe(1)-N(6)	2.0722(19)
Fe-N(Av)	1.987(07)		
N1–Fe1–N2	92.56(8)	N3–Fe1–N2	90.27(8)
N1–Fe1–N3	97.83(8)	N3–Fe1–N4	83.31(8)
N1–Fe1–N4	176.65(8)	N3–Fe1–N5	91.46(8)
N1–Fe1–N5	87.14(8)	N3–Fe1–N6	168.13(8)
N1–Fe1–N6	92.60(8)	N4–Fe1–N6	86.59(8)
N2–Fe1–N4	84.28(8)	N5–Fe1–N4	95.99(8)
N2–Fe1–N5	178.27(8)	N5–Fe1–N6	83.40(7)
N2–Fe1–N6	94.92(8)		

[1]1-X, 1-Y, 1-Z; [2]2-X, 2-Y, 1-Z

Table. **S3** Selected bond distances (Å) and angles (°) for **2** at different temperatures.

Complex **2**$^{250\ K}$			
Fe(1)–N(1)	2.117(2)	Fe(1)–N(4)	2.2500(19)
Fe(1)–N(2)	2.161(2)	Fe(1)–N(5)	2.189(2)
Fe(1)–N(3)	2.178(2)	Fe(1)–N(6)	2.251(2)
Fe-N(Av)	2.191(2)		
N1–Fe1–N2	90.74(8)	N2–Fe1–N6	99.05(7)
N1–Fe1–N3	94.91(8)	N3–Fe1–N4	76.85(8)
N1–Fe1–N4	165.82(8)	N3–Fe1–N5	90.84(8)
N1–Fe1–N5	88.92(8)	N3–Fe1–N6	164.45(8)
N1–Fe1–N6	92.84(8)	N4–Fe1–N5	102.56(8)
N2–Fe1–N3	94.32(8)	N4–Fe1–N6	97.99(8)
N2–Fe1–N4	78.58(8)	N5–Fe1–N6	75.82(7)
N2–Fe1–N5	174.84(8)		

[1]1-X, 1-Y, 1-Z; [2]2-X, -Y, 1-Z

Complex **2**$^{70\ K}$			
Fe(1)–N(1)	1.930(2)	Fe(1)–N(4)	2.078(2)
Fe(1)–N(2)	2.005(2)	Fe(1)–N(5)	2.007(2)
Fe(1)–N(3)	1.978(2)	Fe(1)–N(6)	2.130(2)
Fe-N(Av)	2.021(5)		
N1–Fe1–N2	90.16(8)	N2–Fe1–N6	96.88(8)
N1–Fe1–N3	93.47(9)	N3–Fe1–N4	81.49(9)
N1–Fe1–N4	171.61(9)	N3–Fe1–N5	91.67(8)
N1–Fe1–N5	87.14(8)	N3–Fe1–N6	171.28(8)
N1–Fe1–N6	88.76(8)	N4–Fe1–N5	99.65(8)
N2–Fe1–N3	91.54(8)	N4–Fe1–N6	97.22(8)
N2–Fe1–N4	83.31(8)	N5–Fe1–N6	80.02(8)
N2–Fe1–N5	175.92(8)		

[1]1-X, 1-Y, 1-Z; [2]2-X, -Y, 1-Z

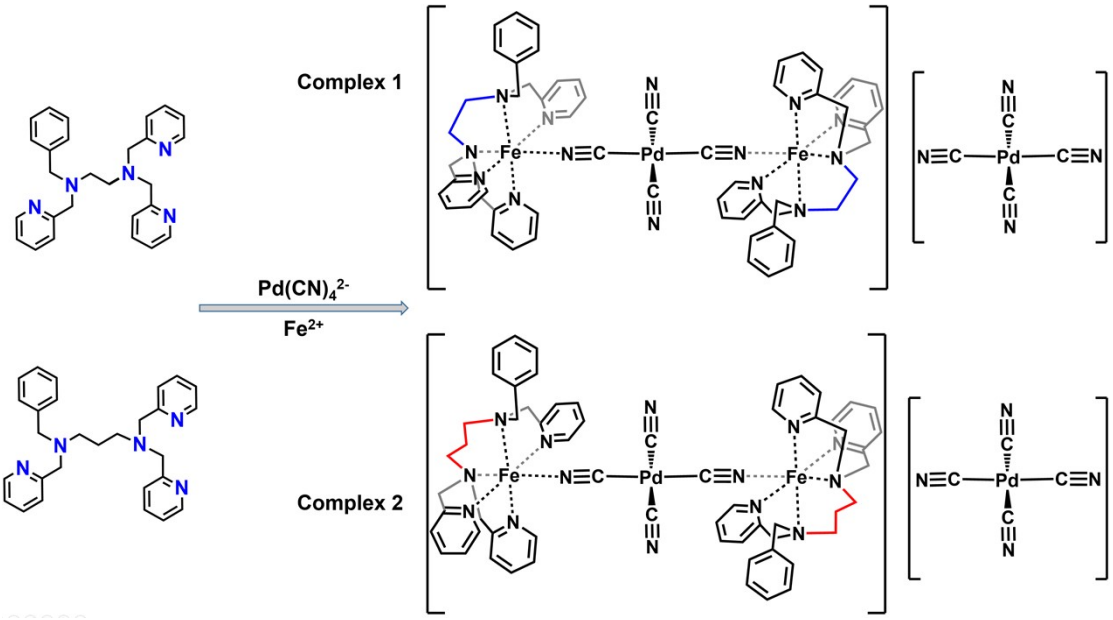

Scheme S1. The synthetic procedures of complexes **1** and **2**.

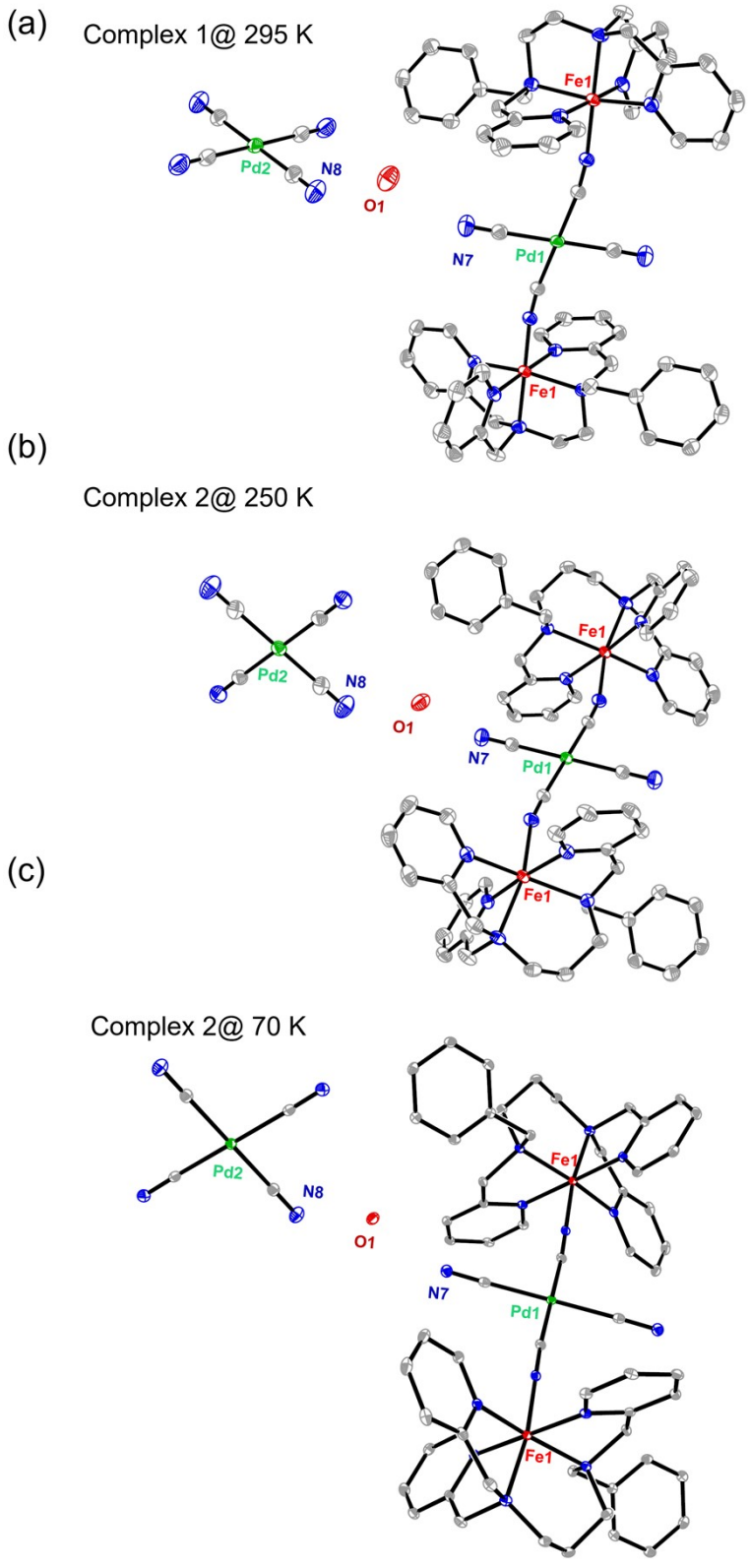

Figure S1. The structures of complexes **1** and **2** at different states, rendered with 30% probability ellipsoids. Hydrogen atoms are omitted for clarity.

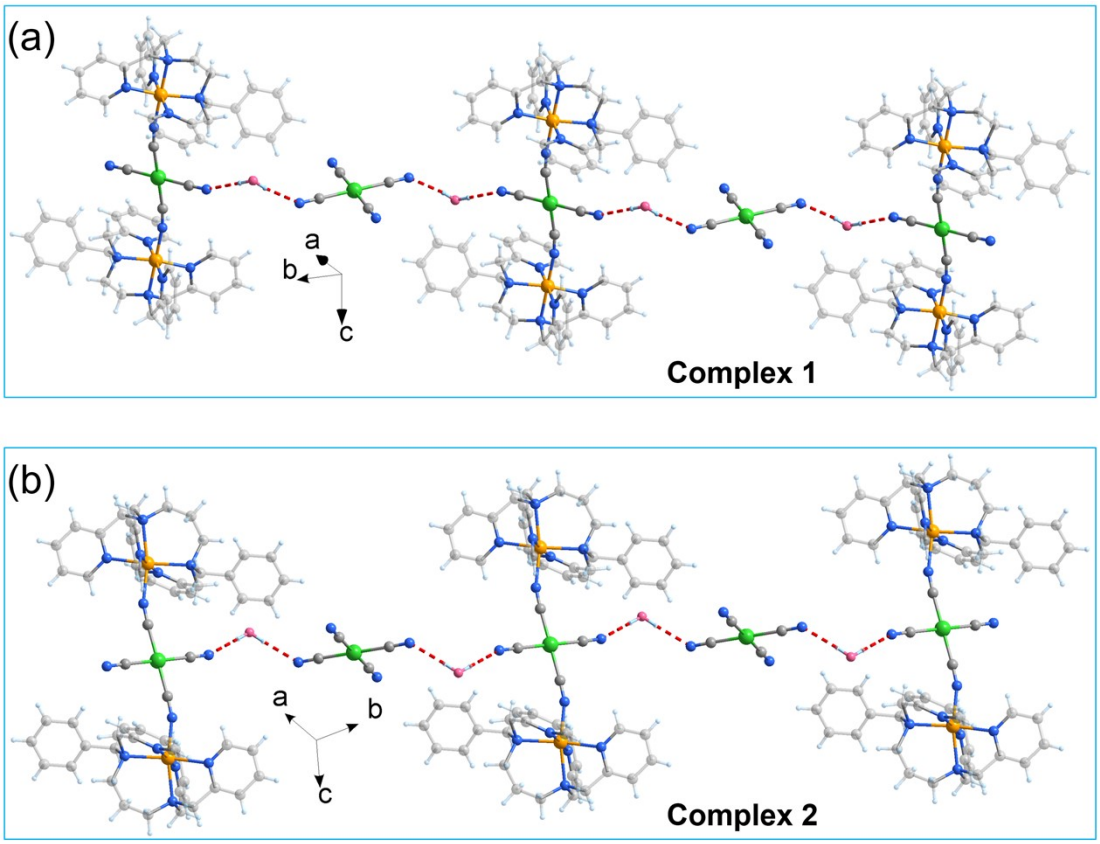

Figure S2. The intermolecular hydrogen bonds are depicted by red dash lines for **1** (a) and **2** (b). Color code: Fe, light orange; Pd, green; C, grey; N, blue; O, red; H, pale blue.

Table S4. The calculated $\chi_M T$ values for **1** and **2** at 298 K according to the Evans' method.

Complex	**1**	**2**
f1(Hz)	1229.1	1163.83
f2(Hz)	1254.6	1253.2
Δf(Hz)	25.5	89.42
$\chi_M T$ (cm^3 mol^{-1} K)	1.71	7.81

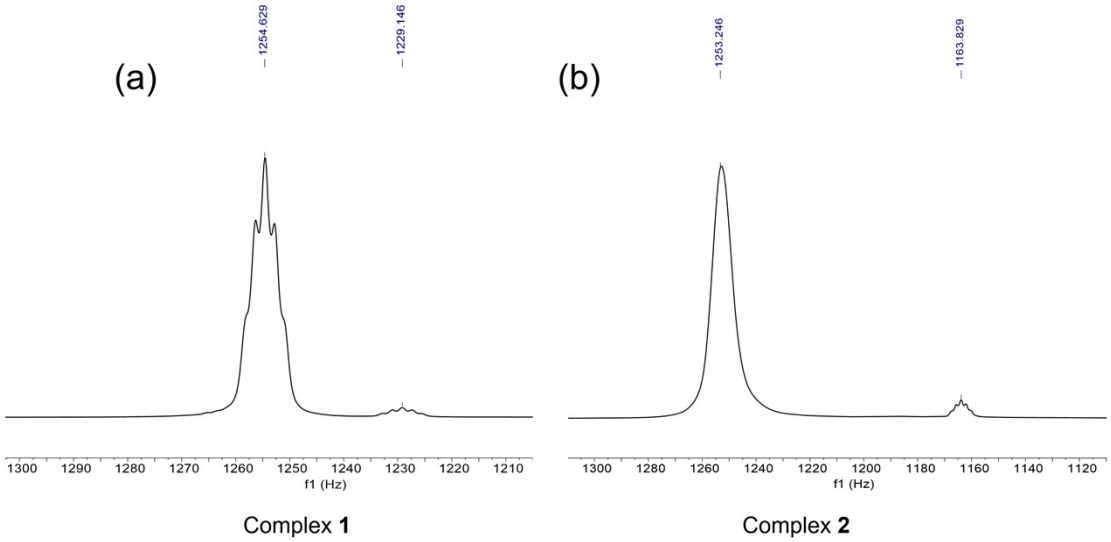

Figure S3. (a) ^{1}H NMR spectrum for complex **1**; (b) ^{1}H NMR spectrum for complex **2**.

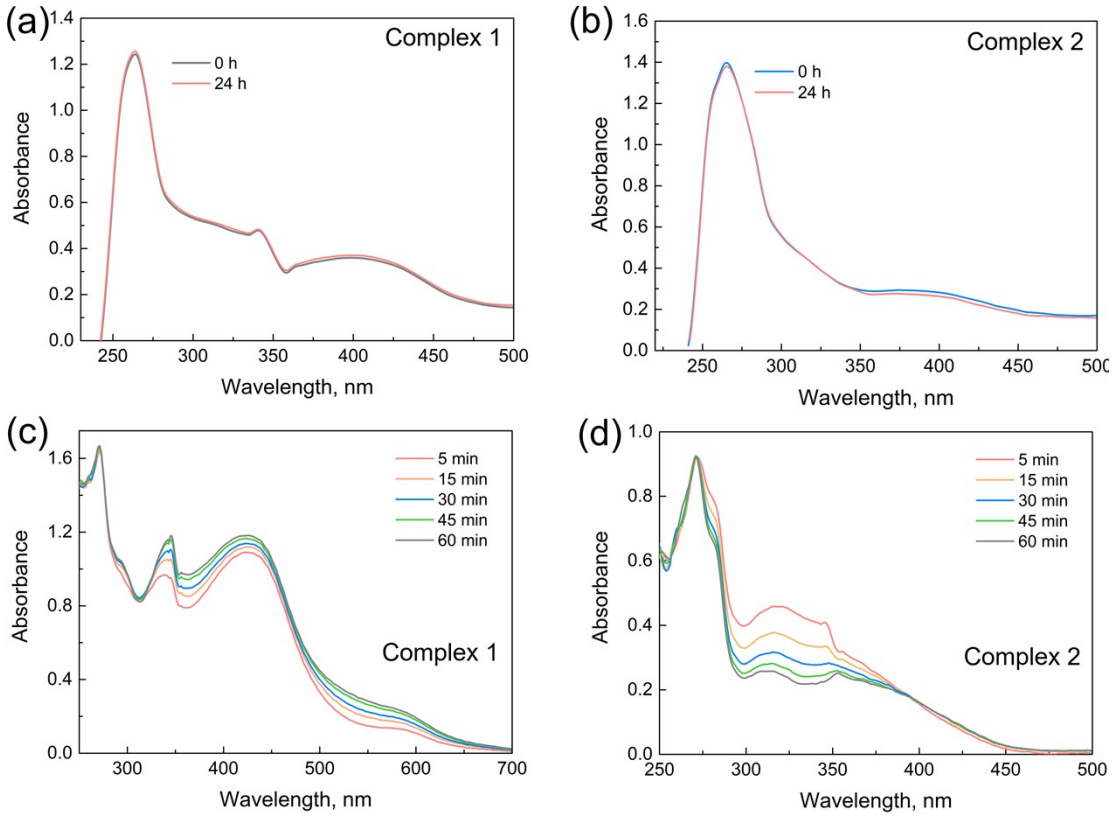

Figure S4. The stability of the synthesized complexes **1** (a) and **2** (b) in DMSO:PBS (2 : 3) were monitored by UV-Vis at 298 K within 24 h; The stability of the complexes **1** (c) and **2** (d) in DMSO was monitored by UV-Vis at a molar ratio of 1:50 (complexes **1** or **2**:ethanethiol) within 1 h.

The stability of organometallic complexes in solution significantly impacts their biological activity. UV-Vis analysis revealed that the basic trend of the spectra of **1** and **2** remained relatively consistent in the presence of DMSO/PBS solution over the 24 h period, suggesting that the complexes are well stabilized in DMSO and PBS solvents. However, in the presence of ethanethiol, the UV-Vis spectra of both complexes exhibited significant changes within one hour, indicating poor stability in ethanethiol and suggesting that decomposition may also occur in vitro in cells.

Table. **S5** IC_{50} values (uM) of complexes toward HepG-2 and HeLa cell lines for 24 h

Complexes	IC_{50} (μM)	
	HepG-2	HeLa
$Fe(ClO_4)_2·6H_2O$	>100	>100
$K_2Pd(CN)_4·3H_2O$	>100	>100
Bztpen	5.72±0.19	3.53±0.15
$\{Fe^{II}_2Bztpen_2[Pd^{II}(CN)_4]_2\}·2H_2O$	3.11 ± 0.19	2.34 ± 0.05
Bztppn	32.25 ± 1.29	28.36 ± 0.68
$\{Fe^{II}_2Bztppn_2[Pd^{II}(CN)_4]_2\}·2H_2O$	13.31 ± 0.54	10.80 ± 0.73

Table. **S6** The distances of C-N···O for **1** and **2** at different states.

Complex **1**	C_{30}–N_7···O_1 (Å)	C_{31}-N_8···O_1 (Å)
295 K	2.94(6)	2.98(8)
Complex **2**	C_{30}–N_7···O_1 (Å)	C_{31}–N_8···O_1 (Å)
250 K	2.98(7)	2.99(2)
70 K	3.02(2)	2.93(8)

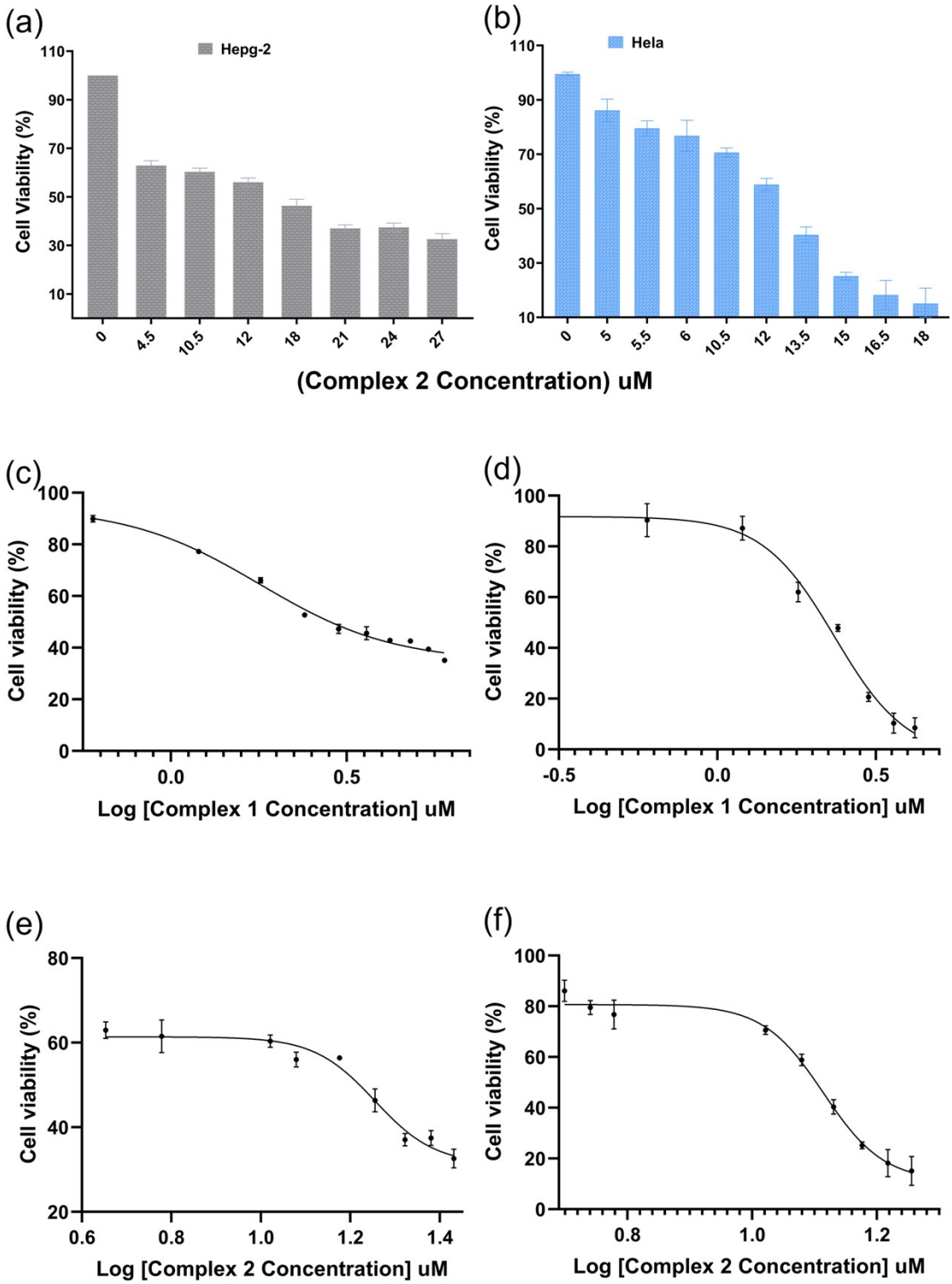

Figure S5. The histogram of complex **2** in dose-dependent cytotoxic effects on the two cells (a) HepG-2 cells, (b) HeLa cells. The fitting curves obtained according to the experimental results are as follows: (c) HepG-2 cells and (d) HeLa cells for complex **1**; (e) HepG-2 cells and (f) HeLa cells for complex **2**.

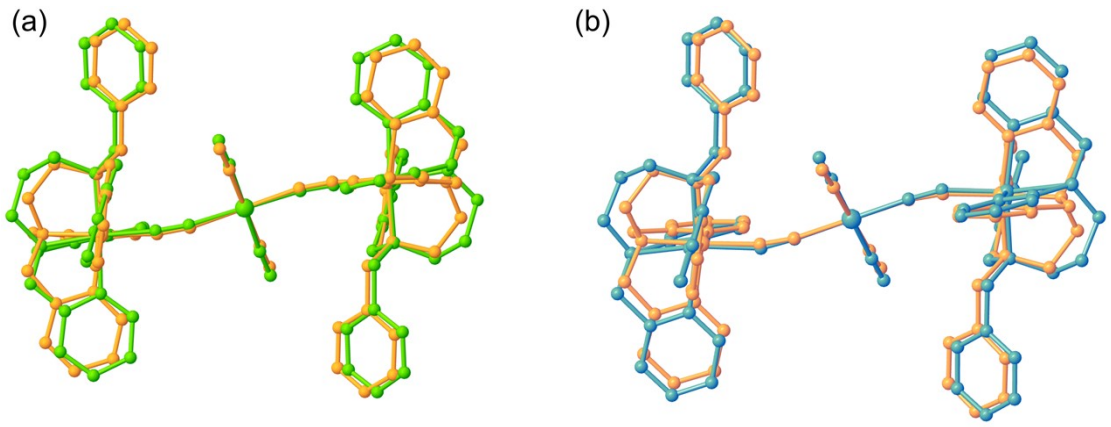

Figure S6. (a) Overlapped structures for **1** (rose) at 300 K with **2** for 70 K (green). (b) Overlapped structures for **1** (rose) at 295 K with **2** (blue) at 250 K.

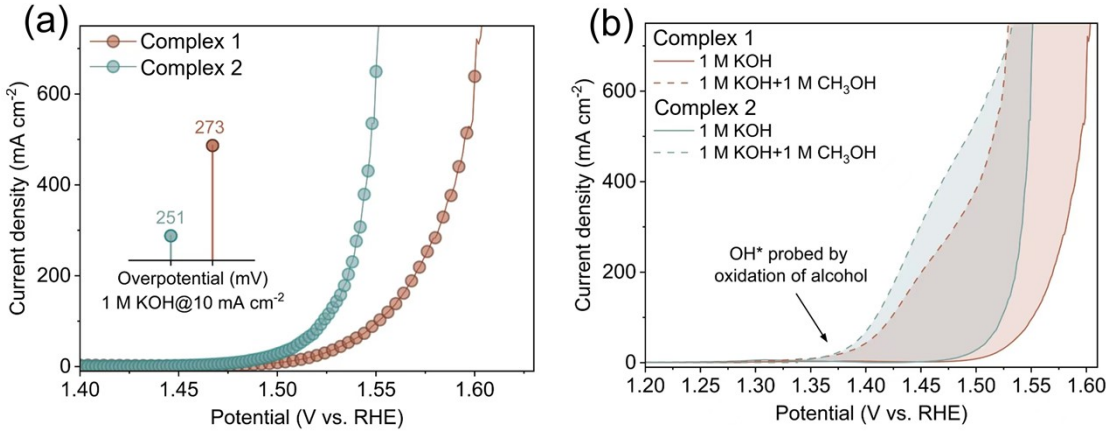

Figure S7. (a) LSV plots for complexes **1** and **2**; (b) CV curves for **1** and **2** at a scan rate of 50 mV s^{-1} performed before and after adding 1 M methanol into 1 M KOH electrolyte. Their performance in oxygen evolution reaction (OER) was assessed using linear sweep voltammetry (LSV) in a 1 M KOH electrolyte. The results show that complexes **1** and **2** require an overpotential of 273 and 251 mV, respectively, to reach a current density of 10 mA cm^{-2} (Figure S5a). Moreover, it is a common sense that the OH * intermediates formed during OER are electrophilic and therefore able to react directly with nucleophiles as methanol. As shown in Figure S5b, the current density increased significantly upon the addition of 1 M methanol, indicating the OH* intermediate was consumed by methanol oxidation. It was demonstrated that complexes **1** and **2** have different electrocatalytic activities.

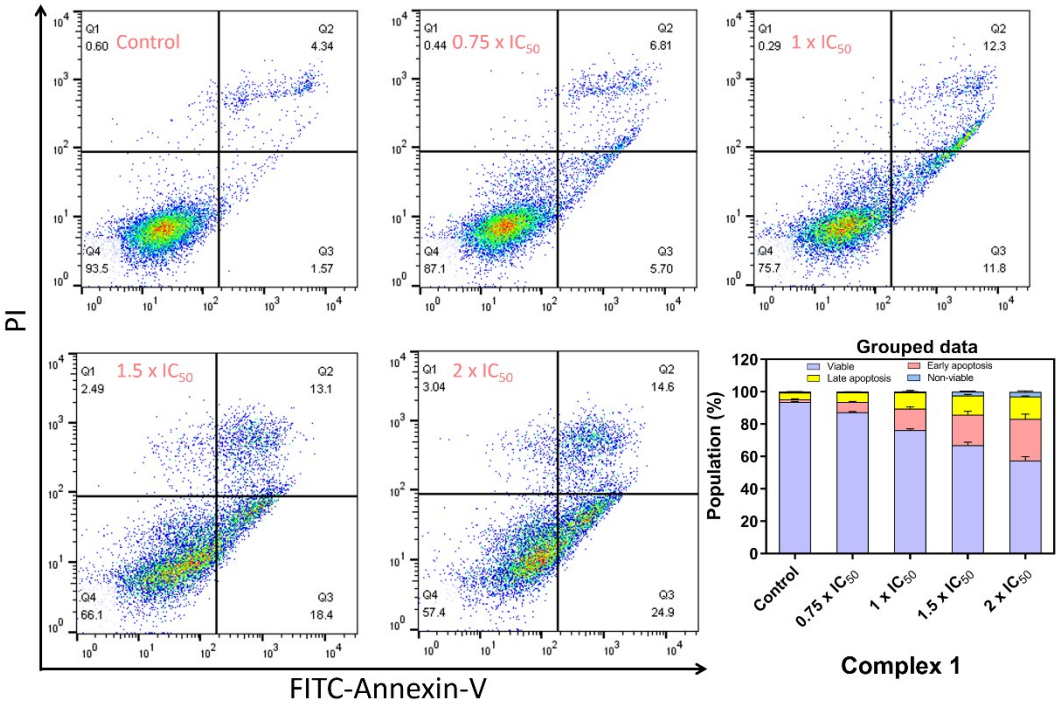

Figure S8. Flow cytometric analysis for apoptotic induction of HepG-2 cells treated with complex **1** for 24 h. Each experiment was performed in triplicate.

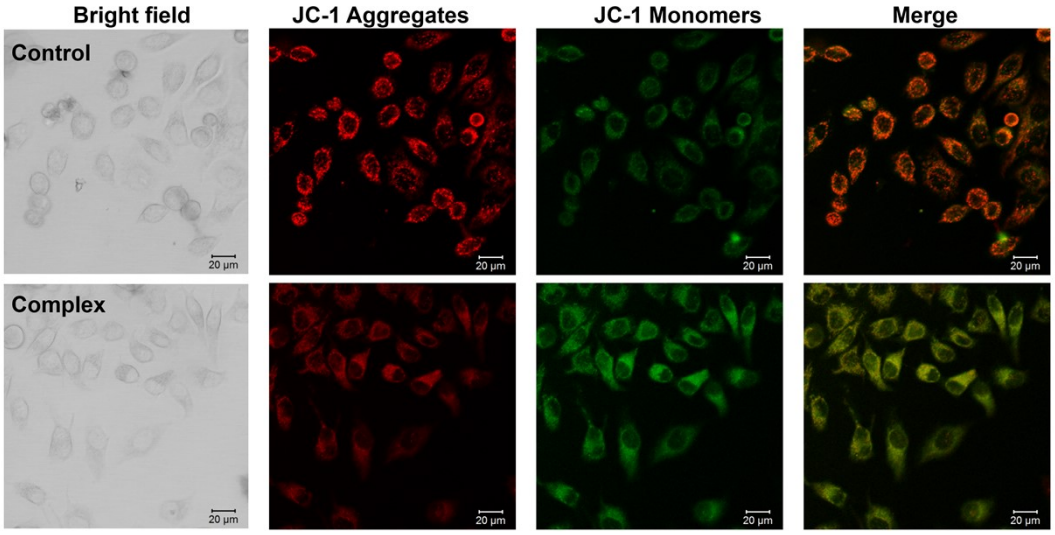

Figure S9. Fluorescence microscopy images of the MMP in control cells and treated cells. Cells were treated with 1 x IC_{50} of complex **1** for 6 h.